Inorganic Chemistry

Article

pubs.acs.org/IC

Conjugation of Organoruthenium(II) 3-(1*H*-Benzimidazol-2-yl)pyrazolo[3,4-*b*]pyridines and Indolo[3,2-*d*]benzazepines to Recombinant Human Serum Albumin: a Strategy To Enhance Cytotoxicity in Cancer Cells

Iryna N. Stepanenko,[†] Angela Casini,[‡,⊥] Fabio Edafe,[‡] Maria S. Novak,[†] Vladimir B. Arion,*[,†] Paul J. Dyson,*[,‡] Michael A. Jakupec,[†] and Bernhard K. Keppler*[,†]

[†]Institute of Inorganic Chemistry, University of Vienna, Währinger Strasse 42, A-1090 Vienna, Austria

[‡]Institut des Sciences et Ingénierie Chimiques, Ecole Polytechnique Fédérale de Lausanne (EPFL), CH-1015 Lausanne, Switzerland

Supporting Information

ABSTRACT: Following our strategy of coupling cyclin-dependent kinase (Cdk) inhibitors with organometallic moieties to improve their physicochemical properties and bioavailability, five organoruthenium complexes (**1c**−**5c**) of the general formula [RuCl(η^6-arene)(L)]Cl have been synthesized in which the arene is 4-formylphenoxyacetyl-η^6-benzylamide and L is a Cdk inhibitor [3-(1*H*-benzimidazol-2-yl)-1*H*-pyrazolo[3,4-*b*]pyridines (**L1**−**L3**) and indolo[3,2-*d*]benzazepines (**L4** and **L5**)]. All of the compounds were characterized by spectroscopic and analytical methods. Upon prolonged standing (2−3 months) at room temperature, the dimethyl sulfoxide (DMSO) solutions of **1c** and $\mathbf{2c}_{-HCl}$ afforded residues, which after recrystallization from EtOH and EtOH/H_2O, respectively, were shown by X-ray diffraction to be *cis*,*cis*-[$Ru^{II}Cl_2(DMSO)_2$(**L1**)]·H_2O and *mer*-[$Ru^{II}Cl(DMSO)_3$(**L2**−H)]·H_2O. Compound **5c**, with a coordinated amidine unit, undergoes *E*/*Z* isomerization in solution. The antiproliferative activities and effects on the cell cycle of the new compounds were evaluated. Complexes **1c**−**5c** are moderately cytotoxic to cancer cells (CH1, SW480, A549, A2780, and A2780cisR cell lines). Therefore, in order to improve their antiproliferative effects, as well as their drug targeting and delivery to cancer cells, **1c**−**5c** were conjugated to recombinant human serum albumin, potentially exploiting the so-called "enhanced permeability and retention" effect that results in the accumulation of macromolecules in tumors. Notably, a marked increase in cytotoxicity of the albumin conjugates was observed in all cases.

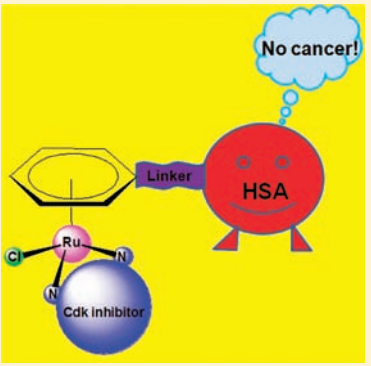

INTRODUCTION

Numerous strategies have been developed for the effective delivery of anticancer drugs to tumor tissue to improve their selectivity and, consequently, to reduce drug side effects.[1−4] By using passive and active targeting strategies, cancer nanotherapeutics, based on polymers (polymeric nanoparticles, micelles, or dendrimers), lipids (liposomes), viruses (viral nanoparticles), and carbon nanotubes, leads to an enhancement of the intracellular concentration of drugs in cancer cells, usually without being blocked by *P*-glycoprotein, a protein responsible for multidrug resistance.[5] These emerging approaches, mainly applied to organic anticancer drugs (e.g., doxorubicin, paclitaxel),[6] have also been used successfully to deliver inorganic drugs, namely, platinum(II) and platinum(IV) complexes.[7]

Serum albumin has been observed to accumulate in solid tumors and, consequently, has been exploited as a drug-delivery system,[8] involving both albumin conjugates for the delivery of anticancer agents and albumin nanoparticles for drug encapsulation. Interestingly, albumin conjugates with methotrexate and a doxorubicin derivative and an albumin paclitaxel nanoparticle (*nab*-paclitaxel; Abraxane) have been evaluated in clinical trials.[8,9] Albumin conjugates of the platinum(II) anticancer drug carboplatin were shown to be as, or more, effective than carboplatin in reducing the tumor size of nude mice bearing human breast tumors and, in some cases, were less toxic.[10] Even if in a less advanced stage of development, an organometallic ruthenium compound has also been conjugated to recombinant human serum albumin (rHSA), with a considerable increase (ca. 20-fold) in cytotoxicity observed (see below).[11,12]

Organometallic ruthenium(II) arene complexes are currently under intensive investigations as anticancer agents,[13−16] with several groups contributing to their design. Within this frame, and as part of our ongoing studies on targeted chemotherapy,[17] involving the development of inhibitors of upregulated receptors and growth factors in cancer cells, we have studied the effect of metal coordination (Ga, Ru, Os, and Cu) of some cyclin-dependent kinase (Cdk) inhibitors (indolo[3,2-*d*]-benzazepines (paullones),[18−23] indolo[3,2-*c*]quinolines,[24] and 3-(1*H*-benzimidazol-2-yl)-1*H*-pyrazolo[3,4-*b*]pyridines[25]) on

Received: August 18, 2011
Published: November 23, 2011

Chart 1. Compounds 1c−5c with Atom Numbering Schemes for NMR Spectroscopic Assignment

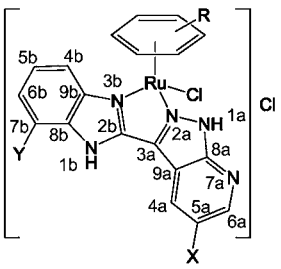

1c (L = L1, X = H, Y = H)
2c (L = L2, X = Br, Y = H)
3c (L = L3, X = Br, Y = CH_2OCH_3)

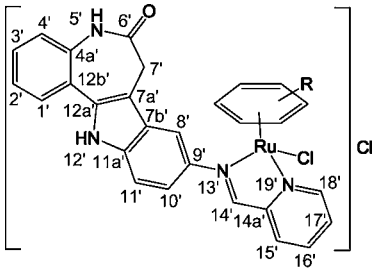

4c (L = L4)

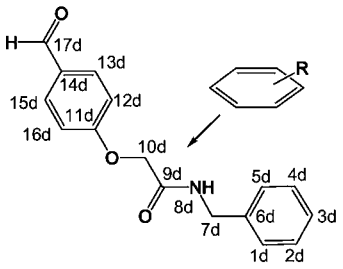

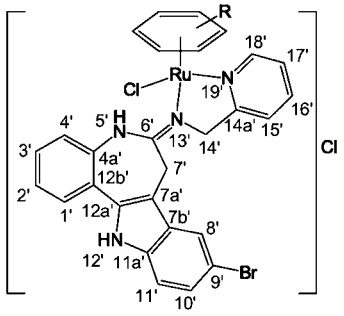

5c (L = L5)

the antiproliferative activity, bioavailability, etc., of the resulting complexes. The promising effects, e.g., increased solubility in physiologically relevant media and synergistic effects from metal and ligand leading to highly cytotoxic species, warrant further efforts in this area.

Herein, we describe the synthesis and characterization of a series of new ruthenium arene complexes of the general formula [RuCl(η^6-arene)(L)]Cl (Chart 1), with a modified arene ligand, 4-formylphenoxyacetyl-η^6-benzylamide, that may be tethered to rHSA and L = 3-(1*H*-benzimidazol-2-yl)-1*H*-pyrazolo[3,4-*b*]pyridines (**L1**−**L3**) and indolo[3,2-*d*]-benzazepines (**L4** and **L5**), which are potential Cdk inhibitors. In order to achieve targeted drug delivery and potentiate the pharmacological effects of the compounds, conjugation of the ruthenium moiety to modified rHSA was realized via hydrazone bond formation according to reported procedure.[10] Interestingly, cleavage of the hydrazone bond under acidic conditions has been exploited for drug release in cancer cells.[26,27] The complexes and their rHSA conjugates have been screened for antiproliferative activity on different human cancer cell lines, and the observed effect on the antitumor activity of tethering these organometallic compounds to rHSA has been discussed.

EXPERIMENTAL SECTION

General Details. 3-(1*H*-Benzimidazol-2-yl)-1*H*-pyrazolo[3,4-*b*]-pyridine (**L1**),[25] 3-(1*H*-benzimidazol-2-yl)-5-bromo-1*H*-pyrazolo[3,4-*b*]pyridine (**L2**),[25] 5-bromo-3-(4-methoxymethyl-1*H*-benzimidazol-2-yl)-1*H*-pyrazolo[3,4-*b*]pyridine (**L3**),[25] 9-(pyridin-2-ylmethylidene)-amino-7,12-dihydroindolo[3,2-*d*][1]benzazepin-6(5*H*)-one (**L4**),[21] 9-bromo-6-(α-picolylamino)-7,12-dihydroindolo[3,2-*d*][1]benzazepine (**L5**),[22] and [RuCl(μ-Cl)(η^6-arene)]$_2$ (where arene = 4-formylphenoxyacetyl-η^6-benzylamide)[11] were prepared according to published protocols (Schemes S1−S3 in the Supporting Informtion). Solvents (ethanol and diethyl ether) were dried using standard procedures. Syntheses of complexes were performed under an argon atmosphere using Schlenk techniques. Elemental analysis (C, H, N, Cl, Br, and S) was performed by the Microanalytical Service of the Institute of Physical Chemistry of the University of Vienna. Electrospray ionization mass spectrometry (ESI-MS) spectra were recorded on a Bruker Esquire 3000 instrument (Bruker Daltonics, Bremen, Germany) using methanolic solutions of the complexes. Values of *m*/*z* are quoted for the species with the highest natural abundance. UV−vis spectra were recorded on a Perkin-Elmer Lambda 20 UV−vis spectrophotometer with samples dissolved in methanol (**1c**−**5c**) and water (**4c** and **5c**) over 24 h. ^{1}H, ^{13}C, and ^{15}N NMR and ^{15}N,^{1}H HSQC, ^{13}C,^{1}H HSQC, ^{13}C,^{1}H HMBC, ^{1}H,^{1}H COSY, ^{1}H,^{1}H TOCSY, and ^{1}H,^{1}H ROESY NMR spectra were measured on a Bruker DPX500 (Ultrashield Magnet) in DMSO-d_6 ([RuCl(μ-Cl)(η^6-arene)]$_2$, [RuCl$_2$(η^6-arene)(DMSO)], **1c**−**5c**, and **2c**$_{-HCl}$), D_2O (for **4c** only ^{1}H NMR), and MeOH-d_4 (for **5c** only ^{1}H and ^{1}H,^{1}H ROESY NMR) using standard pulse programs at 500.32 (^{1}H), 125.81 (^{13}C), and 50.70 (^{15}N) MHz. ^{1}H and ^{13}C shifts are referenced relative to the solvent signals. 2D NMR spectra for **5c** were registered at an equilibrium of *E*/*Z* isomers (for a 2-day-old DMSO-d_6 solution).

Synthesis of [RuCl$_2$(η^6-arene)(DMSO)]. Red crystals of [RuCl$_2$(η^6-arene)(DMSO)]·0.5H_2O suitable for X-ray diffraction study have been obtained from a 1% DMSO/H_2O solution of [RuCl(μ-Cl)(η^6-arene)]$_2$ upon standing at room temperature for 1 month. An upscaled synthesis of [RuCl$_2$(η^6-arene)(DMSO)] along with analytical data is given in the Supporting Information.

Synthesis of [RuCl(η^6-arene)(L1)]Cl (1c). [RuCl(μ-Cl)(η^6-arene)]$_2$·0.5H_2O (149.7 mg, 0.17 mmol) and **L1** (123 mg, 0.52 mmol) were heated in ethanol (25 mL) at 85 °C for 1.5 h. The solvent was evaporated to half of the initial volume, forming a brick-red precipitate that was removed by filtration and dried in vacuo at 50 °C. Yield: 172.8 mg, 75%. Anal. Calcd for $C_{29}H_{24}Cl_2N_6O_3Ru$·0.75H_2O (**1c**·0.75H_2O) (M_r = 690.03 g mol^{-1}): C, 50.48; H, 3.72; N, 12.18; Cl, 10.28. Found: C, 50.57; H, 3.52; N, 12.01; Cl, 10.20. ESI-MS in MeOH (positive): *m*/*z* 605 [**1c** − HCl − Cl]$^+$, 641 [**1c** − Cl]$^+$, 663 [**1c** − HCl + Na]$^+$. ESI-MS in MeOH (negative): *m*/*z* 639 [**1c** − HCl − H]$^-$. UV−vis [MeOH; λ_{max}, nm (ε, M^{-1} cm^{-1})]: 269 (28 807), 283 (31 573), 289 (32 451), sh 333 (17 493). ^{1}H NMR (500.32 MHz, DMSO-d_6): δ 14.82 (br s, 1H, H_{1b}), 9.88 (s, 1H, H_{17d}), 9.12 (d, 1H, *J* = 6.22 Hz, H_{4a}), 8.81 (tr, 1H, *J* = 6.26 Hz, H_{8d}), 8.78 (d, 1H, *J* = 5.19 Hz, H_{6a}), 8.10 (dd, 1H, *J* = 1.84 and 6.82 Hz, H_{4b}), 7.84 (d, 2H, *J* = 8.83 Hz, H_{13d} + H_{15d}), 7.81 (dd, 1H, *J* = 1.94 and 6.10 Hz, H_{7b}), 7.57 (dd, 1H, *J* = 4.62 and 8.21 Hz, H_{5a}), 7.55−7.51 (m, 2H, H_{5b} + H_{6b}), 7.06 (d, 2H, *J* = 8.72 Hz, H_{12d} + H_{16d}), 6.52 (tr, 1H, *J* = 5.83 Hz, H_{2d} or H_{4d}), 6.46 (m, 2H, H_{2d} or H_{4d} + H_{1d} or H_{5d}), 6.33 (br s, 1H, H_{1d} or

dx.doi.org/10.1021/ic201801e | *Inorg. Chem.* 2011, 50, 12669−12679

H_{5d}), 5.99 (t, 1H, J = 5.67 Hz, H_{3d}), 4.59 (s, 2H, H_{10d}), 4.34 (tr, 2H, J = 4.62 Hz, H_{7d}). ^{13}C NMR (125.81 MHz, DMSO-d_6): δ 191.83 (C_{17d}), 168.09 (C_{9d}), 162.69 (C_{11d}), 153.61 (C_{8a}), 150.73 (C_{6a}), 146.74 (C_{2b}), 141.41 (C_{9b}), 134.90 (C_{3a}), 134.58 (C_{8b}), 132.12 (C_{13d} + C_{15d}), 131.51 (C_{4a}), 130.62 (C_{14d}), 125.35 (C_{5b} or C_{6b}), 124.89 (C_{5b} or C_{6b}), 119.38 (C_{5a}), 117.84 (C_{4b}), 115.66 (C_{12d} + C_{16d}), 113.90 (C_{7b}), 111.76 (C_{9a}), 101.93 (C_{6d}), 85.39 (C_{2d} or C_{4d}), 85.09 (C_{2d} or C_{4d}), 83.92 (C_{3d}), 82.67 (C_{1d} or C_{5d}), 82.31 (C_{1d} or C_{5d}), 67.19 (C_{10d}), 40.46 (C_{7d}). ^{15}N NMR (50.70 MHz, DMSO-d_6): δ 89.5 (N_{8d}). Orange crystals of *cis,cis*-[Ru^{II}Cl$_2$(DMSO)$_2$(**L1**)]·H_2O suitable for X-ray diffraction study were grown by recrystallization from ethanol of the product, obtained by the slow evaporation (2−3 months) of a DMSO solution of **1c**.

Synthesis of [RuCl(η^6-arene)(L2)]Cl (2c). *a. Synthesis of* ***2c***$_{-HCl}$·H_2O. [RuCl(μ-Cl)(η^6-arene)]$_2$·0.5H_2O (100 mg, 0.11 mmol) and **L2** (80 mg, 0.26 mmol) were heated in ethanol (20 mL) at 85 °C for 1.5 h. The solvent was evaporated to half of the initial volume, and the yellow precipitate of [RuCl(η^6-arene)(**L2**−H)] (**2c**$_{-HCl}$) was removed by filtration and dried in vacuo at 50 °C. Yield: 151.8 mg, 92%. Anal. Calcd for $C_{29}H_{22}BrClN_6O_3Ru·H_2O$ (**2c**$_{-HCl}$·H_2O) (M_r = 736.97 g mol^{-1}): C, 47.26; H, 3.28; N, 11.40; Cl, 4.81; Br, 10.84. Found: C, 47.53; H, 2.97; N, 11.16; Cl, 4.90; Br, 11.04. ESI-MS in MeOH (positive): m/z 721 [**2c**$_{-HCl}$ + H]$^+$, 743 [**2c**$_{-HCl}$ + Na]$^+$. ESI-MS in MeOH (negative): m/z 719 [**2c**$_{-HCl}$ − H]$^-$. ^{1}H NMR (500.32 MHz, DMSO-d_6): δ 13.89 (br s, 1H, H_{1b}), 9.87 (s, 1H, H_{17d}), 9.03 (tr, 1H, J = 5.96 Hz, H_{8d}), 8.99 (d, 1H, J = 2.06 Hz, H_{4a}), 8.55 (d, 1H, J = 2.04 Hz, H_{6a}), 8.01 (d, 1H, J = 8.02 Hz, H_{4b}), 7.84 (d, 2H, J = 8.76 Hz, H_{13d} + H_{15d}), 7.72 (d, 1H, J = 7.54 Hz, H_{7b}), 7.47 (tr, 1H, J = 7.11 Hz, H_{5b} or H_{6b}), 7.43 (tr, 1H, J = 7.14 Hz, H_{5b} or H_{6b}), 7.13 (d, 2H, J = 8.69 Hz, H_{12d} + H_{16d}), 6.39 (tr, 1H, J = 5.79 Hz, H_{2d} or H_{4d}), 6.25 (d, 1H, J = 5.81 Hz, H_{1d} or H_{5d}), 6.14 (tr, 1H, J = 5.39 Hz, H_{2d} or H_{4d}), 6.06 (m, 2H, H_{1d} or H_{5d} + H_{3d}), 4.75 (dd, 2H, J = 14.49 and 25.44 Hz, H_{10d}), 4.42 (d, 2H, J = 5.94 Hz, H_{7d}). The yellow crystals of *mer*-[Ru^{II}Cl(DMSO)$_3$(**L2**-H)]·H_2O suitable for X-ray diffraction study were grown from a EtOH/H_2O solution of the product, obtained by the slow evaporation (2 months) of a DMSO solution of **2c**$_{-HCl}$.

b. Synthesis of ***2c***·0.5H_2O. A total of 37% HCl (24 mg) was added to **2c**$_{-HCl}$·H_2O (130 mg, 0.18 mmol) in ethanol (20 mL). The suspension was stirred at room temperature for 1 h, and the solvent was removed under reduced pressure. The residue (**2c**) was suspended in diethyl ether, collected by filtration, and dried in vacuo at 50 °C. Yield: 135 mg, 100%. Anal. Calcd for $C_{29}H_{23}BrCl_2N_6O_3Ru·0.5H_2O$ (**2c**·0.5H_2O) (M_r = 764.42 g mol^{-1}): C, 45.57; H, 3.16; N, 10.99; Cl, 9.28. Found: C, 45.75; H, 2.86; N, 10.86; Cl, 8.75. ESI-MS in MeOH (positive): m/z 743 [**2c** − HCl + Na]$^+$. ESI-MS in MeOH (negative): m/z 719 [**2c** − HCl − H]$^-$. UV−vis [MeOH; λ_{max}, nm (ε, M^{-1} cm^{-1})]: 256 (18 146), 300 (24 730), 360 (10 018). ^{1}H NMR (500.32 MHz, DMSO-d_6): δ 14.42 (br s, 1H, H_{1b}), 9.88 (s, 1H, H_{17d}), 9.22 (br s, 1H, H_{4a}), 8.88 (tr, 1H, J = 5.77 Hz, H_{8d}), 8.70 (br s, 1H, H_{6a}), 8.06 (d, 1H, J = 7.23 Hz, H_{4b}), 7.84 (d, 2H, J = 8.83 Hz, H_{13d} + H_{15d}), 7.78 (dd, 1H, J = 1.4 and 7.27 Hz, H_{7b}), 7.50 (m, 2H, H_{5b} + H_{6b}), 7.08 (d, 2H, J = 8.75 Hz, H_{12d} + H_{16d}), 6.46 (tr, 1H, J = 5.76 Hz, H_{2d} or H_{4d}), 6.39 (d, 1H, J = 6.35 Hz, H_{1d} or H_{5d}), 6.35 (tr, 1H, J = 4.21 Hz, H_{2d} or H_{4d}), 6.23 (d, 1H, J = 5.63 Hz, H_{1d} or H_{5d}), 6.04 (t, 1H, J = 5.49 Hz, H_{3d}), 4.63 (dd, 2H, J = 14.34 and 18.53 Hz, H_{10d}), 4.35 (ddd, 2H, J = 6.06, 15.03, and 22.65 Hz, H_{7d}). ^{13}C NMR (125.81 MHz, DMSO-d_6): δ 191.81 (C_{17d}), 168.07 (C_{9d}), 162.68 (C_{11d}), 155.35 (C_{8a}), 150.43 (C_{6a}), 147.32 (C_{2b}), 141.46 (C_{9b}), 134.49 (C_{8b}), 133.23 (C_{3a}), 132.11 (C_{13d} + C_{15d}), 131.16 (C_{4a}), 130.63 (C_{14d}), 125.05 (C_{5b} or C_{6b}), 124.70 (C_{5b} or C_{6b}), 117.64 (C_{4b}), 115.66 (C_{12d} + C_{16d}), 114.25 (C_{5a} or C_{9a}), 113.66 (C_{7b}), 112.69 (C_{5a} or C_{9a}), 101.19 (C_{6d}), 85.26 (C_{2d} or C_{4d}), 84.51 (C_{2d} or C_{4d}), 83.97 (C_{3d}), 83.04 (C_{1d} or C_{5d}), 82.79 (C_{1d} or C_{5d}), 67.19 (C_{10d}), 40.30 (C_{7d}). ^{15}N NMR (50.70 MHz, DMSO-d_6): δ 123.7 (N_{1b}), 88.6 (N_{8d}).

Synthesis of [RuCl(η^6-arene)(L3)]Cl (3c). [RuCl(μ-Cl)(η^6-arene)]$_2$·0.5H_2O (100 mg, 0.11 mmol) and **L3** (91.5 mg, 0.26 mmol) were heated in ethanol (20 mL) at 85 °C for 1 h. The solvent was evaporated to one-third of the initial volume, and the yellow precipitate (**3c**) that formed was removed by filtration and dried in vacuo at 50 °C. Yield: 166 mg, 90%. Anal. Calcd for $C_{31}H_{27}BrCl_2N_6O_4Ru·1.5H_2O$ (**3c**·1.5H_2O) (M_r = 826.49 g mol^{-1}): C, 45.05; H, 3.66; N, 10.17; Cl, 8.58; Br, 9.67. Found: C, 45.31; H, 3.24; N, 10.06; Cl, 8.30; Br, 9.36. ESI-MS in MeOH (positive): m/z 727 [**3c** − HCl − Cl]$^+$, 749 [**3c** − 2HCl + Na]$^+$, 765 [**3c** − Cl]$^+$, 785 [**3c** − HCl + Na]$^+$. ESI-MS in MeOH (negative): m/z 726 [**3c** − 2HCl − H]$^-$, 763 [**3c** − HCl − H]$^-$. UV−vis [MeOH; λ_{max}, nm (ε, M^{-1} cm^{-1})]: 259 (29 157), 302 (37 725), 361 (16 424). ^{1}H NMR (500.32 MHz, DMSO-d_6): δ 14.03 (br s, 1H, H_{1b}), 9.88 (s, 1H, H_{17d}), 9.46 (s, 1H, H_{4a}), 8.88 (tr, 1H, J = 5.65 Hz, H_{8d}), 8.69 (d, 1H, J = 1.74 Hz, H_{6a}), 8.01 (d, 1H, J = 7.85 Hz, H_{4b}), 7.84 (d, 2H, J = 8.81 Hz, H_{13d} + H_{15d}), 7.49 (m, 2H, H_{5b} + H_{6b}), 7.07 (d, 2H, J = 8.68 Hz, H_{12d} + H_{16d}), 6.45 (tr, 1H, J = 5.65 Hz, H_{2d} or H_{4d}), 6.39 (d, 1H, J = 6.08 Hz, H_{1d} or H_{5d}), 6.34 (tr, 1H, J = 4.46 Hz, H_{2d} or H_{4d}), 6.23 (d, 1H, J = 6.05 Hz, H_{1d} or H_{5d}), 6.03 (tr, 1H, J = 5.54 Hz, H_{3d}), 4.87 (dd, 2H, J = 12.39 and 16.13 Hz, H_{10b}), 4.63 (dd, 2H, J = 14.74 and 21.11 Hz, H_{10d}), 4.35 (ddd, 2H, J = 5.88, 15.17, and 19.74 Hz, H_{7d}), 3.39 (s, 3H, H_{11b}). ^{13}C NMR (125.81 MHz, DMSO-d_6): δ 191.81 (C_{17d}), 168.03 (C_{9d}), 162.65 (C_{11d}), 154.91 (C_{8a}), 150.59 (C_{6a}), 147.44 (C_{2b}), 141.69 (C_{9b}), 133.23 (C_{3a}), 132.98 (C_{8b}), 132.10 (C_{13d} + C_{15d}), 131.78 (C_{4a}), 130.62 (C_{14d}), 124.91 (C_{5b} or C_{6b}), 124.63 (C_{5b} or C_{6b}), 124.54 (C_{7b}), 117.22 (C_{4b}), 115.65 (C_{12d} + C_{16d}), 114.31 (C_{5a} or C_{9a}), 112.74 (C_{5a} or C_{9a}), 101.36 (C_{6d}), 85.24 (C_{2d} or C_{4d}), 84.56 (C_{2d} or C_{4d}), 84.34 (C_{3d}), 83.26 (C_{1d} or C_{5d}), 82.99 (C_{1d} or C_{5d}), 70.13 (C_{10b}), 67.17 (C_{10d}), 57.97 (C_{11b}), 40.30 (C_{7d}). ^{15}N NMR (50.70 MHz, DMSO-d_6): δ 123.8 (N_{1b}), 88.9 (N_{8d}).

Synthesis of [RuCl(η^6-arene)(L4)]Cl (4c). [RuCl(μ-Cl)(η^6-arene)]$_2$·0.5H_2O (100.3 mg, 0.11 mmol) and **L4** (80.03 mg, 0.23 mmol) were heated in ethanol (15 mL) at 85 °C for 3 h. After cooling to room temperature, the reaction mixture was filtered and evaporated to a minimum volume. The addition of diethyl ether resulted in the precipitation of a brown product, which was removed by filtration and dried in vacuo. Yield: 163 mg, 87%. Anal. Calcd for $C_{38}H_{31}Cl_2N_5O_4Ru·2H_2O$ (**4c**·2H_2O) (M_r = 829.69 g mol^{-1}): C, 55.01; H, 4.25; N, 8.44. Found: C, 55.04; H, 4.10; N, 8.41. ESI-MS in MeOH (positive): m/z 758 [**4c** − Cl]$^+$, 723 [**4c** − HCl − Cl]$^+$. ESI-MS in MeOH (negative): m/z 756 [**4c** − HCl − H]$^-$, 720 [**4c** − 2HCl − H]$^-$. UV−vis [MeOH; λ_{max}, nm (ε, M^{-1} cm^{-1})]: 218 (63 208), sh 251 (42 884), sh 261 (42 361), sh 281 (36 827), sh 289 (35 680), 315 (33 347), 375 (12 616). UV−vis [H_2O; λ_{max}, nm (ε, M^{-1} cm^{-1})]: sh 216 (54 985), 288 (35 202), sh 313 (27 554), 381 (10 800). ^{1}H NMR (500.32 MHz, DMSO-d_6): δ 12.08 (s, 1H, H_{12}'), 10.21 (s, 1H, H_5'), 9.87 (s, 1H, H_{17d}), 9.61 (d, 1H, J = 5.25 Hz, H_{18}'), 8.98 (s, 1H, H_{14}'), 8.78 (t, 1H, J = 5.94 Hz, H_{8d}), 8.32−8.27 (m, 2H, H_{15}' + H_{16}'), 8.08 (d, 1H, J = 1.93 Hz, H_8'), 7.85 (d, 2H, J = 8.84 Hz, H_{13d} + H_{15d}), 7.84 (m, 1H, H_1' or H_{17}'), 7.80 (dd, 1H, J = 1.15 and 7.73 Hz, H_1' or H_{17}'), 7.77 (dd, 1H, J = 2.05 and 8.64 Hz, H_{10}'), 7.64 (d, 1H, J = 8.66 Hz, H_{11}'), 7.44 (t, 1H, J = 7.77 Hz, H_3'), 7.32 (m, 2H, H_2' + H_4'), 7.11 (d, 2H, J = 8.72 Hz, H_{12d} + H_{16d}), 6.17 (t, 1H, J = 5.96 Hz, H_{3d}), 5.95−5.91 (m, 2H, H_{2d} + H_{4d}), 5.76−5.71 (m, 2H, H_{1d} + H_{5d}), 4.69 (dd, 2H, J = 14.94 and 20.42 Hz, H_{10d}), 4.29 (ddd, 2H, J = 5.74, 15.36, and 33.98 Hz, H_{7d}), 3.61 (s, 2H, H_7'). ^{13}C NMR (DMSO-d_6, 125.81 MHz): δ 191.78 (C_{17d}), 171.94 (C_6'), 168.25 (C_{9d}), 166.55 (C_{14}'), 162.83 (C_{11d}), 156.61 (C_{18}'), 155.53 (C_{14a}'), 145.69 (C_9'), 140.41 (C_{16}'), 138.08 (C_{11a}'), 136.19 (C_{4a}'), 135.43 (C_{12a}'), 132.16 (C_{13d} + C_{15d}), 130.66 (C_{14d}), 129.76 (C_{15}'), 129.05 (C_3'), 128.75 (C_{17}'), 127.58 (C_1'), 126.68 (C_{7b}'), 124.29 (C_2'), 122.89 (C_4'), 122.83 (C_{12b}'), 118.86 (C_{10}'), 115.69 (C_{12d} + C_{16d}), 112.55 (C_{11}'), 111.22 (C_8'), 108.91 (C_{7a}'), 102.16 (C_{6d}), 88.49 (C_{1d} or C_{5d}), 88.37 (C_{3d}), 85.86 (C_{2d} or C_{4d}; C_{1d} or C_{5d}), 85.80 (C_{2d} or C_{4d}; C_{1d} or C_{5d}), 85.11 (C_{2d} or C_{4d}), 67.28 (C_{10d}), 39.93 (C_{7d}), 32.32 (C_7'). ^{15}N NMR (DMSO-d_6, 50.70 MHz): δ 116.38 (N_5'), 110.02 (N_{12}'), 88.51 (N_{8d}).

Synthesis of [RuCl(η^6-arene)(L5)]Cl (5c). [RuCl(μ-Cl)(η^6-arene)]$_2$·0.5H_2O (108 mg, 0.12 mmol) and **L5** (102.3 mg, 0.25 mmol) were heated in ethanol (15 mL) at 85 °C for 3 h. After cooling to room temperature, the reaction mixture was filtered and evaporated to a minimum volume. Diethyl ether was added, and the yellow-brown precipitate was collected and dried in vacuo. Yield: 185 mg, 87%. Anal. Calcd for $C_{38}H_{32}BrCl_2N_5O_3Ru·H_2O$ (**5c**·H_2O) (M_r = 876.59 g mol^{-1}): C, 52.07; H, 3.91; N, 7.99. Found: C, 51.97; H, 3.95; N, 7.73. ESI-MS in MeOH (positive): m/z 825 [**5c** − Cl]$^+$, 789 [**5c** −

dx.doi.org/10.1021/ic201801e | *Inorg. Chem.* 2011, 50, 12669−12679

Table 1. Crystal Data and Details of Data Collection for $[RuCl_2(\eta^6\text{-arene})(DMSO)]\cdot 0.5H_2O$, L2·DMSO, *cis,cis*-$[Ru^{II}Cl_2(DMSO)_2(L1)]\cdot H_2O$, and *mer*-$[Ru^{II}Cl(DMSO)_3(L2-H)]\cdot H_2O$

	$[RuCl_2(\eta^6\text{-arene})DMSO]\cdot 0.5H_2O$	L2·DMSO	$[Ru^{II}Cl_2(DMSO)_2(L1)]\cdot H_2O$	$[Ru^{II}Cl(DMSO)_3(L2-H)]\cdot H_2O$
empirical formula	$C_{18}H_{22}Cl_2NO_{4.5}RuS$	$C_{15}H_{14}BrN_5OS$	$C_{17}H_{23}Cl_2N_5O_3RuS_2$	$C_{19}H_{27}BrClN_5O_4RuS_3$
fw	528.40	392.28	581.49	702.07
space group	$P\bar{1}$	$P2_1/c$	$P\bar{1}$	$P2_1/c$
a [Å]	8.5676(4)	8.5399(4)	7.8726(6)	11.8408(9)
b [Å]	10.8811(4)	10.2371(6)	11.1638(9)	12.9306(10)
c [Å]	11.4797(5)	18.5633(11)	13.0422(10)	17.9286(2)
α [deg]	72.819(2)		97.546(5)	
β [deg]	89.461(3)	94.712(4)	94.461(5)	108.707(4)
γ [deg]	77.030(2)		106.202(5)	
V [Å^3]	994.49(7)	1617.39(15)	1083.29(15)	2600.0(3)
Z	2	4	2	4
λ [Å]	0.710 73	0.710 73	0.710 73	0.710 73
ρ_{calcd} [g cm^{-3}]	1.765	1.611	1.194	2.520
cryst size [mm^3]	0.20 × 0.04 × 0.02	0.38 × 0.14 × 0.08	0.10 × 0.08 × 0.08	0.20 × 0.10 × 0.01
T [K]	100	100	100	100
μ [mm^{-1}]	1.189	2.682	1.194	2.520
R1[a]	0.0461	0.0428	0.0519	0.0355
wR2[b]	0.1264	0.0978	0.1390	0.0817
GOF[c]	1.094	0.965	1.005	0.994

[a] $R1 = \sum||F_o| - |F_c||/\sum|F_o|$. [b] $wR2 = \{\sum[w(F_o^2 - F_c^2)^2]/\sum[w(F_o^2)^2]\}^{1/2}$. [c] $GOF = \{\sum[w(F_o^2 - F_c^2)^2]/(n-p)\}^{1/2}$, where n is the number of reflections and p is the total number of parameters refined.

HCl − Cl]$^+$. ESI-MS in MeOH (negative): m/z 823 [**5c** − HCl − H]$^-$, 786 [**5c** − 2HCl − H]$^-$. UV−vis [MeOH; λ_{max}, nm (ε, M^{-1} cm^{-1})]: sh 230 (43 177), 268 (44 722), 319 (21 929). UV−vis [H_2O; λ_{max}, nm (ε, M^{-1} cm^{-1})]: sh 217 (32 402), sh 237 (26 864), 273 (28 107), 314 (13 462).

a. NMR Characterization of E/Z Isomers in DMSO-d_6. ^{1}H NMR (500.32 MHz, DMSO-d_6): *E*-isomer, δ 12.05 (s, 1H, H_{12}'), 9.87 (s, 1H, H_{17d}), 9.11 (d, 1H, J = 5.56 Hz, H_{18}'), 9.07 (s, 1H, H_5'), 8.69 (t, 1H, J = 5.9 Hz, H_{8d}), 8.22 (d, 1H, J = 1.66 Hz, H_8'), 8.09 (t, 1H, J = 7.86 Hz, H_{16}'), 7.85 (d, 2H, J = 8.42 Hz, H_{13d} + H_{15d}), 7.83 (d, 1H, J = 7 Hz, H_1'), 7.65 (d, 1H, J = 7.87 Hz, H_{15}'), 7.59 (t, 1H, J = 6.64 Hz, H_{17}'), 7.46 (m, 2H, H_3' + H_{11}'), 7.37 (d, 1H, J = 8.2 Hz, H_{10}'), 7.34 (m, 2H, $H_{2(E)}'$ + $H_{2(Z)}'$), 7.26 (d, 1H, J = 7.94 Hz, H_4'), 7.09 (d, 2H, J = 8.72 Hz, H_{12d} + H_{16d}), 6.03 (t, 1H, J = 5.74 Hz, H_{2d} or H_{4d}), 5.95 (t, 1H, J = 5.73 Hz, H_{2d} or H_{4d}), 5.90 (d, 1H, J = 6.05 Hz, H_{1d} or H_{5d}), 5.84 (d, 1H, J = 18.4 Hz, H_{14}'), 5.83 (t, 1H, J = 5.59 Hz, H_{3d}), 5.77 (d, 1H, J = 5.88 Hz, H_{1d} or H_{5d}), 5.22 (d, 1H, J = 17.07 Hz, H_{14}'), 4.77 (d, 1H, J = 13.21 Hz, H_7'), 4.64 (s, 2H, H_{10d}), 4.09 (d, 2H, J = 6.09 Hz, H_{7d}), 3.47 (d, 1H, J = 15.25 Hz, H_7'). ^{1}H NMR (500.32 MHz, DMSO-d_6): *Z* isomer, δ 11.85 (s, 1H, H_{12}'), 9.88 (s, 1H, H_{17d}), 9.67 (s, 1H, H_5'), 9.03 (d, 1H, J = 5.39 Hz, H_{18}'), 8.89 (t, 1H, J = 5.93 Hz, H_{8d}), 8.32 (d, 1H, J = 1.69 Hz, H_8'), 7.96 (t, 1H, J = 7.65 Hz, H_{16}'), 7.87 (d, 2H, J = 8.72 Hz, H_{13d} + H_{15d}), 7.81 (d, 1H, J = 7.76 Hz, H_1'), 7.72 (d, 1H, J = 8.26 Hz, H_4'), 7.51 (m, 2H, H_3' + H_{17}'), 7.41 (m, 2H, H_{11}' + H_{15}'), 7.34 (m, 2H, $H_{2(E)}'$ + $H_{2(Z)}'$), 7.22 (dd, 1H, J = 1.8 and 8.52 Hz, H_{10}'), 7.15 (d, 2H, J = 8.69 Hz, H_{12d} + H_{16d}), 6.27 (t, 1H, J = 5.79 Hz, H_{2d} or H_{4d}), 6.14 (t, 1H, J = 5.66 Hz, H_{2d} or H_{4d}), 6.06 (d, 1H, J = 5.84 Hz, H_{1d} or H_{5d}), 5.98 (m, 2H, H_{3d} + H_{1d} or H_{5d}), 5.16 (d, 1H, J = 18.15 Hz, H_{14}'), 4.99 (d, 1H, J = 18.27 Hz, H_{14}'), 4.92 (d, 1H, J = 13.99 Hz, H_7'), 4.76 (s, 2H, H_{10d}), 4.42 (ddd, 2H, J = 5.86, 14.81, and 47.62 Hz, H_{7d}), 3.69 (d, 1H, J = 14.18 Hz, H_7'). ^{13}C NMR (125.81 MHz, DMSO-d_6): *E* isomer, δ 191.82 (C_{17d}), 168.16 (C_{9d}), 167.64 (C_6'), 162.75 (C_{11d}), 161.52 (C_{14a}'), 155.37 (C_{18}'), 140.07 (C_{16}'), 136.50 (C_{11a}'), 135.78 (C_{4a}'), 135.35 (C_{12a}'), 132.17 (C_{13d} + C_{15d}), 130.67 (C_{14d}), 129.39 (C_3'), 128.66 (C_{7b}'), 127.75 (C_1'), 125.43 (C_2', C_{10}', or C_{17}'), 125.34 (C_2', C_{10}', or C_{17}'), 124.74 (C_2' or C_{10}'), 122.31 (C_4'), 122.19 (C_{12b}'), 121.23 (C_8' or C_{15}'), 121.18 (C_8' or C_{15}'), 115.67(C_{12d} + C_{16d}), 114.18 (C_{11}'), 112.61 (C_9'), 107.21 (C_{7a}'), 103.28 (C_{6d}), 90.03 (C_{2d} or C_{4d}), 89.49 (C_{2d} or C_{4d}), 82.49 (C_{1d} or C_{5d}), 81.97 (C_{1d} or C_{5d}), 80.78 (C_{3d}), 67.27 (C_{10d}), 62.52 (C_{14}'), 40.71 (C_{7d}), 24.02 (C_7'). ^{13}C NMR (125.81 MHz, DMSO-d_6): *Z* isomer, δ 191.82 (C_{17d}), 168.36 (C_{9d}), 165.62 (C_6'), 162.87 (C_{11d}), 160.54 (C_{14a}'), 155.24 (C_{18}'), 139.65 (C_{16}'), 136.44 (C_{11a}'), 136.13 (C_{4a}'), 133.89 (C_{12a}'), 132.17 (C_{13d} + C_{15d}), 130.67 (C_{14d}), 128.75 (C_{7b}'), 128.48 (C_3'), 127.55 (C_1'), 125.15 (C_2', C_{10}', or C_{17}'), 124.98 (C_2', C_{10}', or C_{17}'), 124.85 (C_2', C_{10}', or C_{17}'), 123.57 (C_4'), 123.08 (C_8'), 122.56 (C_{12b}'), 121.12 (C_{15}'), 115.73 (C_{12d} + C_{16d}), 113.37 (C_{11}'), 111.69 (C_9'), 109.13 (C_{7a}'), 102.16 (C_{6d}), 88.96 (C_{2d} or C_{4d}), 88.29 (C_{2d} or C_{4d}), 83.19 (C_{1d} or C_{5d}), 82.28 (C_{1d}, C_{5d}, or C_{3d}), 81.74 (C_{1d}, C_{5d}, or C_{3d}), 67.41 (C_{10d}), 62.68 (C_{14}'), 40.71 (C_{7d}), 32.77 (C_7'). ^{15}N NMR (50.70 MHz, DMSO-d_6): *E* isomer, δ 109.42 (N_{12}'), 107.95 (N_5'), 88.39 (N_{8d}). ^{15}N NMR (50.70 MHz, DMSO-d_6): *Z* isomer, δ 107.95 (N_{12}'), 107.46 (N_5'), 88.39 (N_{8d}).

b. NMR Characterization of E/Z Isomers in MeOH-d_4. ^{1}H NMR (500.32 MHz, MeOH-d_4): *E* isomer, δ 9.87 (s, 1H, H_{17d}), 9.42 (s, 1H, H_5'), 9.08 (d, 1H, J = 5.13 Hz, H_{18}'), 8.11 (d, 1H, J = 1.72 Hz, H_8'), 8.06 (t, 1H, J = 7.76 Hz, H_{16}'), 7.88 (d, 2H, J = 8.81 Hz, H_{13d} + H_{15d}), 7.84 (dd, 1H, J = 1.46 and 7.58 Hz), 7.70 (d, 1H, J = 7.79 Hz, H_{15}'), 7.54 (t, 1H, J = 6.66 Hz, H_{17}'), 7.45−7.33 (m, 3H), 7.29 (m, 2H, H_4' + 1H), 7.12 (d, 2H, J = 8.76 Hz, H_{12d} + H_{16d}), 5.94 (t, 1H, J = 5.81 Hz, H_{2d}, H_{3d}, or H_{4d}), 5.78 (d, 1H, J = 17.1 Hz, H_{14}'), 5.75−5.72 (m (d + t), 2H), 5.66 (t, 1H, J = 5.67 Hz, H_{2d}, H_{3d}, or H_{4d}), 5.56 (d, 1H, J = 5.88 Hz, H_{1d} or H_{5d}), 5.29 (d, 1H, J = 17.01 Hz, H_{14}'), 4.90 (d, 1H, J = 15.08 Hz, H_7'), 4.64 (d, 2H, J = 2.99 Hz, H_{10d}), 4.13 (dd, 2H, J = 13.07 and 50.57 Hz, H_{7d}), 3.29 (d, 1H, J = 14.81 Hz, H_7') [based only on the ^{1}H,^{1}H ROESY NMR plot and due to absence of N*H* signals (except H_5), protons H_1, H_2, H_3, H_{10}, and H_{11} (5H) were not assigned]. ^{1}H NMR (500.32 MHz, MeOH-d_4): *Z* isomer, δ 9.84 (s, 1H, H_{17d}), 8.99 (d, 1H, J = 5.24 Hz, H_{18}'), 8.35 (d, 1H, J = 1.73 Hz, H_8'), 7.92 (t, 1H, J = 7.68 Hz), 7.85 (d, 2H, J = 8.78 Hz, H_{13d} + H_{15d}), 7.79 (dd, 1H, J = 1.44 and 7.82 Hz), 7.61 (d, 1H, J = 8.11 Hz), 7.49 (t, 1H, J = 6.95 Hz), 7.45−7.33 (m, 4H, H_{15}' + H_{17}' + 2H), 7.23 (dd, 1H, J = 1.86 and 8.6 Hz), 7.18 (d, 2H, J = 8.74 Hz, H_{12d} + H_{16d}), 6.21 (t, 1H, J = 5.75 Hz, H_{2d}, H_{3d}, or H_{4d}), 6.05 (t, 1H, J = 5.68 Hz, H_{2d}, H_{3d}, or H_{4d}), 6.03 (d, 1H, J = 5.99 Hz, H_{1d} or H_{5d}), 5.92 (d, 1H, J = 6.13 Hz, H_{1d} or H_{5d}), 5.89 (t, 1H, J = 5.55 Hz, H_{2d}, H_{3d}, or H_{4d}), 5.11 (d, 1H, J = 18.09 Hz, H_{14}'), 4.97 (d, 1H, J = 14.08 Hz, H_7'), 4.92 (d, 1H, J = 17.77 Hz, H_{14}'), 4.82 (m, 2H, H_{10d}), 4.59 (m, 2H, H_{7d}), 3.69 (d, 1H, J = 13.95 Hz, H_7') [based only on the ^{1}H,^{1}H ROESY NMR plot and due to the absence of N*H* signals, protons H_1, H_2, H_3, H_4, H_{10}, H_{11}, and H_{16} (7H) were not assigned].

dx.doi.org/10.1021/ic201801e | *Inorg. Chem.* 2011, 50, 12669−12679

Crystal Structure Determinations. X-ray diffraction measurements were performed on a Bruker X8 APEX II CCD diffractometer. Single crystals were positioned at 35, 40, 35, and 35 mm from the detector, and 1335, 752, 2025, and 1096 frames were measured, each for 60, 50, 60, and 60 s over a 1° scan width for $[RuCl_2(\eta^6\text{-arene})(DMSO)]\cdot 0.5H_2O$, **L2**·DMSO, *cis,cis*-$[Ru^{II}Cl_2(DMSO)_2(\mathbf{L1})]\cdot H_2O$, and *mer*-$[Ru^{II}Cl(DMSO)_3(\mathbf{L2}-H)]\cdot H_2O$, respectively. The data were processed using *SAINT* software.[28] Crystal data, data collection parameters, and structure refinement details are given in Table 1. The structures were solved by direct methods and refined by full-matrix least-squares techniques. Non-H atoms were refined with anisotropic displacement parameters. H atoms were inserted into calculated positions and refined with a riding model. One of the chloride ligands in $[RuCl_2(\eta^6\text{-arene})\text{-DMSO}]\cdot 0.5H_2O$ was found to be disordered over two positions with sof = 0.57:0.43. The structure solution was achieved with *SHELXS-97* and refinement with *SHELXL-97*,[29] and graphics were produced with *ORTEP-3*.[30]

Conjugation of Complexes to rHSA. rHSA (50 mg mL^{-1}) was purchased as a 5% solution in phosphate-buffered saline (PBS; containing 4 mM sodium caprylate and 4 mM acetyltryptophan; New Century Pharmaceuticals Inc., Huntsville, AL) and was purified by ultrafiltration using Centricon YM-10 (Amicon Bioseparations, Millipore Corp.) against the modification buffer (PBS, pH 7.4). The concentration of the protein was determined using the Bradford assay (Bio-Rad) using bovine serum albumin as the reference protein. The purified protein (33.2 mg of protein mL^{-1}) was shaken with a solution of succinyl HCl terephthalic hydrazine (SHTH; 10 equiv) in DMF (50 μL) for 16 h at room temperature such that the DMF volume did not exceed 5% (v/v). The reaction mixture was then ultrafiltered against the conjugation buffer (100 mM MES, 0.9% NaCl, pH 6.0), and the concentration of the modified protein was determined using the Bradford assay. The modified protein solution (7 mg of protein mL^{-1}) was added to solutions of the complex (**1c**−**5c**) in order to achieve a 3:1 metal/protein ratio and shaken for 6 h at room temperature. Afterward, the protein mixture solution was desalted and restored in PBS as described above. The concentration of conjugated rHSA−complex conjugate in PBS was determined using the Bradford assay to be 2×10^{-4} M protein.

Matrix-Assisted Laser Desorption Ionization Time-of-Flight Mass Spectrometry (MALDI-TOF-MS) Analyses. The rHSA samples were characterized by MALDI-TOF-MS using an Axima CFR-Plus (Shimadzu Biotech) mass spectrometer. The samples were prepared using the dried droplet method with freshly prepared sinapinic acid [20 mg mL^{-1} in CH_3CN/H_2O/trifluoroacetic acid (50:49.9:0.1)] as the matrix solution. The protein sample solution (0.5 mL, series of 1:10 dilutions) was mixed on the target with the matrix solution (0.5 mL) and allowed to air-dry. The MS spectra were recorded in the m/z 100−80 000 range in a positive linear mode. External calibration was carried out with a mixture of five proteins. Data interpretation was performed using the *Kompact v2.4.3* software.

Cell Culture and Inhibition of Cell Growth. Human CH1 (ovarian carcinoma) cells were donated by Lloyd R. Kelland, CRC Centre for Cancer Therapeutics, Institute of Cancer Research, Sutton, U.K. Human A549 (nonsmall cell lung carcinoma) and SW480 (colon carcinoma) cells were provided by Brigitte Marian, Institute of Cancer Research, Department of Medicine I, Medical University of Vienna, Austria. Cells were grown as adherent cultures in 75 cm^2 flasks (Iwaki) in Minimal Essential Medium (MEM) supplemented with 10% heat-inactivated fetal bovine serum, 1 mM sodium pyruvate, 1% nonessential amino acids (100×), and 2 mM L-glutamine (all from Sigma-Aldrich Austria) without antibiotics at 37 °C under a moist atmosphere containing 5% CO_2 and 95% air. Cytotoxicity was determined by the MTT assay [MTT = 3-(4,5-dimethyl-2-thiazolyl)-2,5-diphenyl-2*H*-tetrazolium bromide]. For this purpose, cells were harvested from culture flasks by trypsinization and seeded in aliquots of 100 μL $well^{-1}$ into 96-well microculture plates (Iwaki) in the following cell densities to ensure exponential growth of untreated controls throughout drug exposure: 4×10^3 (A549), 1×10^3 (CH1) and 2.5×10^3 (SW480) cells $well^{-1}$. Cells were allowed for 24 h to settle and resume exponential growth and were then exposed to the test compounds by the addition of 100 μL $well^{-1}$ aliquots of appropriate dilutions in complete culture medium. For this purpose, DMSO stocks of the compounds were diluted in the medium such that the actual DMSO content in the tested solutions did not exceed 0.5%. After exposure for 96 h, the medium was replaced with 100 μL $well^{-1}$ RPMI 1640 medium plus 20 μL $well^{-1}$ MTT dissolved in PBS (5 mg mL^{-1}). After 4 h, the medium/MTT mixture was replaced with 150 μL $well^{-1}$ DMSO to dissolve the formazan precipitate formed by viable cells. Optical densities at 550 nm (corrected for unspecific absorbance at 690 nm) were measured with a microplate reader (Tecan Spectra Classic) to yield relative quantities of viable cells as percentages of untreated controls, and 50% inhibitory concentrations (IC_{50}) were calculated by interpolation. Evaluation is based on at least three independent experiments, each comprising triplicate samples.

Human A2780 and A2780cisR ovarian carcinoma cell lines were obtained from the European Centre of Cell Cultures (ECACC, Salisbury, U.K.) and maintained in a culture as described by the provider. The cells were routinely grown in RPMI 1640 medium containing 10% fetal calf serum and antibiotics at 37 °C and 6% CO_2. For evaluation of the growth inhibition tests, the cells were seeded in 96-well plates (Costar, Integra Biosciences, Cambridge, MA) and grown for 24 h in the complete medium. The stock solutions of the ruthenium complexes were prepared by dissolving the compounds in 1 mL of DMSO to reach a concentration of 10^{-2} M. They were then diluted in a RPMI medium and added to the wells (100 μL) to obtain a final concentration ranging between 0 and 200 μM. DMSO at comparable concentrations did not show any effects on cytotoxicity. rHSA−ruthenium conjugates (2×10^{-4} M) were directly added to the cell culture to achieve a final concentration ranging from 0 up to 100 μM. After 72 h of incubation at 37 °C, 20 μL of a solution of MTT in PBS (2 mg mL^{-1}) were added to each well, and the plates were then incubated for 2 h at 37 °C. The medium was then aspirated, and DMSO (100 μL) was added to dissolve the precipitate. The absorbance of each well was measured at 580 nm using a 96-well multiwell-plate reader (iEMS Reader MF, Labsystems, Bioconcept, Switzerland) and compared to the values of control cells incubated without complexes. The IC_{50} values for the inhibition of cell growth were determined by fitting the plot of the percentage of surviving cells against the drug concentration using a sigmoidal function (*Origin v7.5*).

Cell Cycle Analysis. The effects of the compounds on the cell cycle of human cancer cells were studied by flow cytometric analysis of the relative DNA content of cells. For this purpose, CH1 cells were harvested from culture flasks by using trypsin, seeded in complete MEM into 90-mm Petri dishes (1×10^6 cells $dish^{-1}$), and allowed to recover for 24 h. Cells were then exposed for 24 h to the test compounds (diluted from DMSO stocks with complete medium), collected by scratching, washed with PBS, and stained with 5 μg mL^{-1} propidium iodide overnight. The fluorescence of 2.5 or 3.0×10^4 cells per sample was measured with a FACSCalibur instrument, and the obtained histograms were analyzed with *CellQuest Pro* software (both from Becton Dickinson, Franklin Lakes, NJ). At least two independent experiments were performed for each setting.

RESULTS AND DISCUSSION

Synthesis and Characterization of Complexes. The metal-free ligands (**L1**−**L5**) and $[RuCl(\mu\text{-}Cl)(\eta^6\text{-arene})]_2$ (where arene is 4-formylphenoxyacetyl-η^6-benzylamide) were prepared via various multistep reaction pathways. The 3-(1*H*-benzimidazol-2-yl)-1*H*-pyrazolo[3,4-*b*]pyridines were obtained in seven (**L1**), eight (**L2**), or eleven (**L3**) steps by modified literature procedures (Scheme S1 in the Supporting Information).[25] Indolo[3,2-*d*]benzazepines (**L4** and **L5**) were synthesized in five steps, as described elsewhere (Scheme S2 in the Supporting Information).[21,22] $[RuCl(\mu\text{-}Cl)(\eta^6\text{-arene})]_2$ was obtained in four steps, as reported in the literature (Scheme S3 in the Supporting Information).[11] Finally, the ligands (**L1**−

Chart 2. *E* (left) and *Z* (right) Isomers of 5c

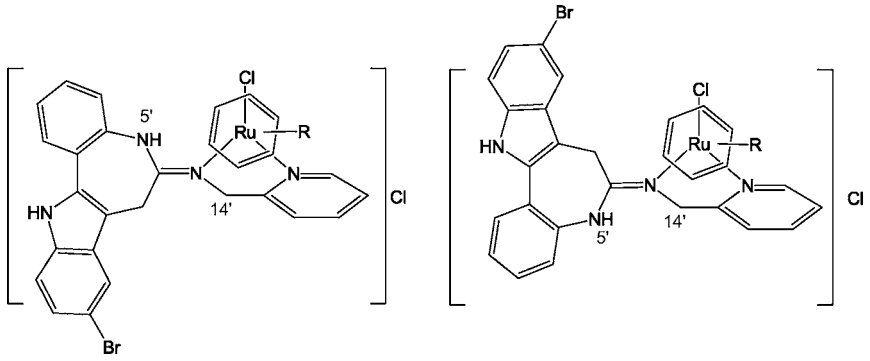

Chart 3. Coordination of L3 [7b−L3 (left) and 4b′−L3 (right) Tautomers]

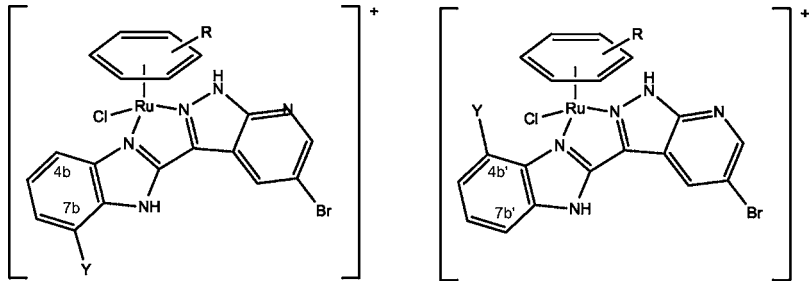

L5) were reacted with the ruthenium(II) dimer in a 2:1 molar ratio in ethanol under reflux to give [RuCl(η^6-arene)(L)]Cl (**1c** and **3c**−**5c**) in quantitative yield. In the case of **L2**, the reaction carried out under similar conditions resulted in the formation of [RuCl(η^6-arene)(**L2**−H)] (**2c**$_{-HCl}$), which was further converted into **2c** by acidification with HCl.

ESI-MS spectra of **1c**−**5c** in MeOH show peaks corresponding to ions $[M - Cl]^+$ and $[M - HCl - H]^-$, confirming their structures. Additional peaks resulting from the loss of the chlorido ligand along with concomitant deprotonation of the organic ligands, namely, $[M - HCl - Cl]^+$ and $[M - 2HCl - H]^-$, are observed with peaks attributed to $[M - HCl + Na]^+$ ions.

NMR spectra of **1c**−**4c** and **2c**$_{-HCl}$ show one set of signals, whereas complex **5c** was found to undergo *E*/*Z* isomerization at the exocyclic amidine bond (C_6'═N_{13}') in solution (Chart 2). Analogous behavior was documented recently for [MCl(η^6-*p*-cymene)(**L5**)]Cl (where M = Ru, Os).[21] The full assignment of proton, nitrogen, and carbon resonances for [RuCl(μ-Cl)(η^6-arene)]$_2$ and **1c**−**5c** is given in Tables S1−S6 in the Supporting Information.

The *E*/*Z* isomerization of **5c** is solvent-dependent; the relative intensities of the two signal sets for **5c** in DMSO-d_6 change from 1:0.6 immediately after dissolution to 1:2.4 at equilibrium after 48 h. According to the ^{1}H,^{1}H ROESY NMR plot, the predominant signal set at equilibrium belongs to the *Z* isomer, which shows H_{14}',H_5' cross-peaks (Figure S7 in the Supporting Information). In MeOH-d_4, the *E*/*Z* equilibrium for **5c** is reached faster than that in DMSO-d_6 and the relative abundance of *E* and *Z* isomers changes from 1:0.5 to 1:0.36 in 3 h (1:0.33 after 24 h). The dominant *E* isomer was identified due to the ^{1}H,^{1}H ROESY NMR couplings of H_5' with arene protons (H_{1d}−H_{5d}), as well as H_7' with H_{14}'. The *Z* isomer shows cross-peaks of H_7' with arene protons (H_{1d}−H_{5d}). It should be noted that only one N*H* (H_5') signal, originating from the *E* isomer, is present in the ^{1}H NMR spectrum after dissolution in MeOH-d_4. This dissapears gradually (the intensity decreases by a factor of 10.8 after 3 h, 65 after 9 h to zero after 14 h).

Dissociation of the complexes may be excluded because the chemical shifts of both signal sets differed from that of metal-free **L5** (Table S5 in the Supporting Information). Moreover, these two sets were not affected by excess chloride ions in MeOH-d_4, providing evidence against solvolysis of the Ru−Cl bond. Thus, at equilibrium the *Z* isomer dominates in DMSO-d_6, whereas the *E* isomer dominates in MeOH-d_4, in line with reported data for [MCl(η^6-*p*-cymene)(**L5**)]Cl.[21]

The coordination of the ligands (**L1**−**L5**) to the ruthenium(II) arene moiety results in significant changes to the resonances of both the ligands and η^6-arene. For instance, significant upfield shifts were observed for the resonances of the η^6-phenyl fragment protons H_{1d}, H_{5d}, H_{2d}, and H_{4d} of 4-formylphenoxyacetyl-η^6-benzylamide in **4c** and **5c** (*E* isomer) compared to those in [RuCl(μ-Cl)(η^6-arene)]$_2$, whereas they are shifted downfield in **1c**−**3c**, **2c**$_{-HCl}$, and **5c** (*Z* isomer); the resonance of the H_{3d} proton in all complexes is shifted downfield.

The number of signals in the ^{1}H NMR spectra of **1c**−**3c** and **2c**$_{-HCl}$ is in agreement with their C_1 symmetry, and five-membered chelate cycle formation via the nitrogens N_{2a} and N_{3b} is evident. The ^{1}H,^{1}H ROESY NMR coupling of H_{1b} (14.03 ppm) with the CH_2 group (H_{10b} at 4.87 ppm) in **3c** indicates stabilization of the **7b**−**L3** tautomer (Chart 3). The same coordination mode was reported for [MCl(η^6-*p*-cymene)-(**L3**)]Cl (where M = Ru, Os).[25]

Upon coordination of **L1**−**L3** to the ruthenium(II) arene moiety, significant shifts were observed for the resonances of the benzimidazole ring protons: H_{1b} [by 1.71 (**L1**), 0.7 (**L2** in **2c**$_{-HCl}$), 1.23 (**L2** in **2c**), 0.78 (**L3**) ppm] and H_{4b} [by 0.29 ppm in **3c**; the H_{4b} and H_{7b} proton resonances in **L1** and **L2** (at 7.54 and 7.75−7.77 ppm) were not assigned; the proton H_{4b} gives a peak at 8.1, 8.06, and 8.01 ppm for **1c**, **2c**, and **2c**$_{-HCl}$,

dx.doi.org/10.1021/ic201801e | *Inorg. Chem.* 2011, 50, 12669−12679

respectively]. The resonance for the pyrazolopyridine proton H_{1a} (the proton nearest to the metal center) was not detected in DMSO-d_6 in **1c**−**3c**.

The signals originating from benzimidazole *C*H C_{4b} and quaternary C_{7b} carbons in **3c** and the **7b**−**L3** tautomer are observed near the same positions [C_{4b} at 118.97 (**7b**−**L3**) and 117.22 (**3c**) ppm; C_{7b} at 122.95 (**7b**−**L3**) and 124.54 (**3c**) ppm] and differ significantly from those in the **4b′**−**L3** tautomer (quaternary C_{4b}′ at 129.38 ppm; *C*H carbon C_{7b}′ at 111.17 ppm). These data provide further evidence of **7b**−**L3** tautomer coordination to ruthenium in **3c**.

The coordination of **L4** results in a significant downfield shift for the resonances corresponding to H_8′ (by 0.28 ppm), H_{10}′ (by 0.43 ppm), and H_{18}′ (by 0.88 ppm). Carbon resonances C_{14}′ (166.55 ppm) and C_{18}′ (156.61 ppm) also differ relative to the free ligand, by 8.18 and 6.14 ppm, respectively, indicating bidentate paullone coordination via the pyridine (N_{19}′) and azomethine nitrogens (N_{13}′) to ruthenium with the formation of a five-membered chelate ring. The azepine methylene protons H_7′ of **4c** display no diastereotopic splitting (singlet at 3.61 ppm), as was the case for free **L4** and [MCl(η^6-*p*-cymene)(**L4**)]Cl (M = Ru, Os).[21]

Ligand **L5** (with an endocyclic double bond C_6′=N_5′) adopts a configuration with an exocyclic double bond C_6′=N_{13}′ upon coordination and protonated N_5′ instead of the N_{13}′ atom (Chart 4). As a result, the triplet corresponding to H_{13}′ at 7.81 ppm for **L5** disappears and proton H_5′ of **5c** emerges as a singlet at 9.67 (*Z* isomer) and 9.07 (*E* isomer) ppm. Because of this rearrangement of the ligand tautomeric form, a large ^{15}N shift for the protonated amidine N atom from 77.4 (**L5**) to 107.46 (*Z* isomer) and 107.95 ppm (*E* isomer) is observed (Table S4 in the Supporting Information).

Chart 4. Tautomers of L5

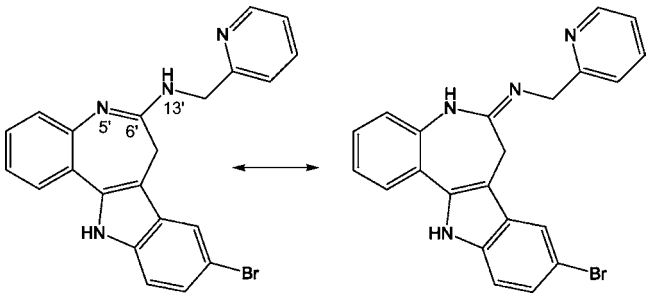

The methylene groups of the azepine ring [H_7′; 3.47 and 4.77 ppm (*E* isomer); 3.69 and 4.92 ppm (*Z* isomer)] and α-picolylamine moiety [H_{14}′; 5.22 and 5.84 ppm (*E* isomer) and 4.99 and 5.16 ppm (*Z* isomer)] in **5c** show diastereotopic splitting, as reported for [MCl(η^6-*p*-cymene)(**L5**)]Cl,[21] whereas for the **L5** proton H_7′, resonance, in accordance with fast inversion of the seven-membered azepine ring, was found at 3.41 ppm as a singlet and proton H_{14}′ gives rise to a doublet at 4.51 ppm.

The **L5** ligand in **5c** undergoes significant downfield shifts for H_7′ (by 0.06−1.51 ppm), H_{14}′ (by 0.48−1.33 ppm), and H_{18}′ [by 0.52 (*Z* isomer) and 0.6 (*E* isomer) ppm]. Carbon signals C_{14}′ and C_{18}′ were shifted compared to those of the free ligand by 15.24 (*Z* isomer), 15.08 (*E* isomer), 5.57 (*Z* isomer), and 5.7 (*E* isomer) ppm, indicating bidentate paullone coordination via the nitrogens N_{19}′ and N_{13}′ to the ruthenium center, as reported for [MCl(η^6-*p*-cymene)(**L5**)]Cl.[21]

Cross-peaks of high intensity in the ^{1}H,^{1}H ROESY NMR spectra of **1c**−**3c** between the η^6-arene ring protons H_{1d}, H_{5d}, H_{2d}, and H_{4d} and the nearest benzimidazole H_{4b} proton reveal strong couplings. Thus, the 4-formylphenoxyacetyl-η^6-benzylamide in **1c**−**3c** in a DMSO-d_6 solution must be oriented in such a manner that its substituent *R*, or H_{3d}, lies above the chelate ring (Figure S8 in the Supporting Information). The closest η^6-arene ring pyrazolopyridine proton H_{1a} was not observed in **1c**−**3c** in DMSO-d_6. Similar solution structures were suggested for [MCl(η^6-*p*-cymene)(L)]Cl (M = Ru, Os; L = **L1**−**L3**).[25] Note that orientation of the cymene ring with the isopropyl group above the chelate ring is the preferred orientation in the crystal structures.[25]

The structures of **4c** and **5c** in DMSO-d_6 were determined from ^{1}H,^{1}H ROESY NMR plots and were compared with the solution and X-ray structures of [MCl(η^6-*p*-cymene)(L)]Cl.[21] The X-ray structures of *p*-cymene analogue complexes facilitate the interpretation of the solution structures of **4c** and **5c** (*E*/*Z* isomers). The cross-peak originating from H_8′,H_{14}′ is more intense than that of H_{10}′,H_{14}′ (i.e., the H_{14}′ proton is closer to H_8′ than H_{10}′), thus the chelating moiety in **4c** is rotated out of the plane of the paullone indole ring with a torsion angle $\Theta_{C14'-N13'-C9'-C10'} > 90°$, as observed in [MCl($\eta^6$-*p*-cymene)(**L4**)]Cl[21] (Figure S9 in the Supporting Information). The orientation of the 4-formylphenoxyacetyl-η^6-benzylamide group in **4c** may be deducted from the intensity of the ^{1}H−^{1}H ROESY cross-peaks between protons of the paullone ligand (H_8′, H_{10}′, and H_{18}′) and those of the η^6-arene ring. Despite the absence of cross-peaks of H_{14}′ with H_{3d} and H_{7d} and the same intensities of the cross-peaks between H_{18}′ and η^6-arene ring protons, the most intense couplings, H_8′, H_{10}′ with H_{1d}, H_{5d}, assume the η^6-arene ring orientation preferably with a substituent *R* above the chelate ring away from the pyridine ring. Couplings H_8′,H_{7d} and H_{10}′,H_{7d} are in accordance with the proposed η^6-arene orientation (Figure S10 in the Supporting Information).

The arene ligand orientation with its substituent above the chelate ring was also observed in a DMSO-d_6 solution for **5c**. For example, the H_{14}′ protons of both isomers oriented toward the arene ring (at 5.16 ppm for the *Z* isomer and at 5.22 ppm for the *E* isomer) show couplings with H_{7d} (Figure S11 in the Supporting Information). The intensity of the cross-peaks in the ^{1}H,^{1}H ROESY NMR plot between protons of the paullone, H_{18}′, and the η^6-arene ring indicates a strong coupling between H_{18}′ and H_{1d}/H_{5d}. This observation is in agreement with the η^6-arene ring orientation with the substituent above the chelate ring toward the pyridine ring (Figure S12 in the Supporting Information). In the *Z* isomer, the azepine methylene group (H_7′) is directed toward the arene ring and shows the ^{1}H,^{1}H ROESY NMR cross-peaks with η^6-arene ring protons. In the *E* isomer, it points away from the arene ring, and as result, there are no ^{1}H−^{1}H ROESY couplings with H_{1d}−H_{5d} (Figure S13 in the Supporting Information).

Solid-State Structures. The molecular structures of [$RuCl_2$(η^6-arene)(DMSO)], where η^6-arene = 4-formylphenoxyacetyl-η^6-benzylamide, and **L2**·DMSO are shown in Figures S14 and S15 in the Supporting Information, respectively.

The structures of *cis*,*cis*-[$Ru^{II}Cl_2(DMSO)_2$(**L1**)]·H_2O and *mer*-[$Ru^{II}Cl(DMSO)_3$(**L2**−H)]·H_2O are shown in Figure 1. Selected bond distances and angles are quoted in the legend. The complex *cis*,*cis*-[$Ru^{II}Cl_2(DMSO)_2$(**L1**)]·H_2O crystallized in the triclinic centrosymmetric space group $P\bar{1}$ and *mer*-[$Ru^{II}Cl(DMSO)_3$(**L2**−H)]·H_2O in the monoclinic space

dx.doi.org/10.1021/ic201801e | *Inorg. Chem.* 2011, 50, 12669−12679

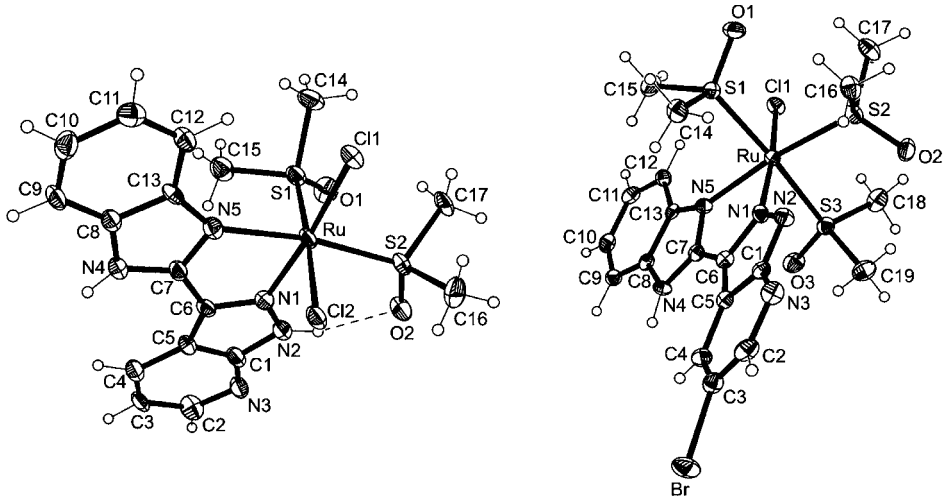

Figure 1. ORTEP views of *cis,cis*-[$Ru^{II}Cl_2(DMSO)_2$(**L1**)] with an intramolecular hydrogen bond N2−H···O2 [N2−H 0.88, H···O2 2.151, N2···O2 2.822 Å, N2−H···O2 132.6°] (left) and *mer*-[$Ru^{II}Cl(DMSO)_3$(**L2**−H)] (right) and thermal ellipsoids drawn at the 50% probability level. Selected bond lengths (Å) and angles (deg): (a) *cis,cis*-[$Ru^{II}Cl_2(DMSO)_2$(**L1**)], Ru−N1 2.057(4), Ru−N5 2.137(4), Ru−Cl1 2.4141(14), Ru−Cl2 2.4604(14), Ru−S1 2.2352(15), Ru−S2 2.2598(14) Å, N1−Ru−N5 76.95(17), $\Theta_{N1-C6-C7-N5}$ 6.7(7)°; (b) *mer*-[$Ru^{II}Cl(DMSO)_3$(**L2**−H)], Ru−N1 2.049(4), Ru−N5 2.135(3), Ru−Cl1 2.4228(11), Ru−S1 2.2878(11), Ru−S2 2.2834(12), Ru−S3 2.3485(11) Å, N1−Ru−N5 77.98(13), $\Theta_{N1-C6-C7-N5}$ −3.5(6)°.

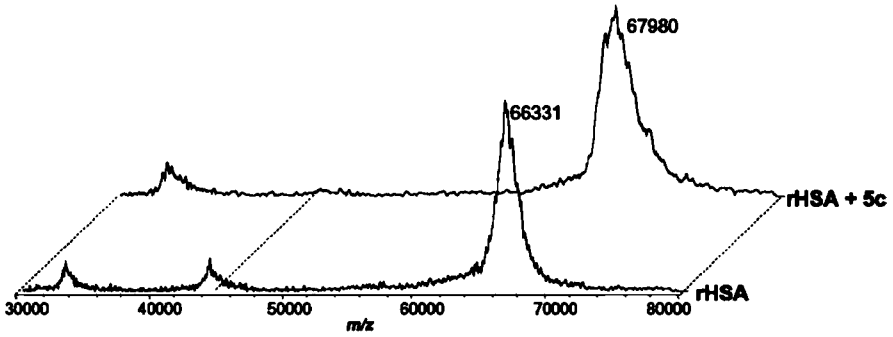

Figure 2. MALDI-TOF-MS spectra of rHSA and rHSA−**5c** conjugate.

group $P2_1/c$. The ruthenium center in both complexes displays a distorted octahedral coordination geometry. In *cis,cis*-[$Ru^{II}Cl_2(DMSO)_2$(**L1**)]·H_2O, a bidentate neutral ligand **L1**, one DMSO, and one chloride ligand are bound to ruthenium(II) in the equatorial plane and one chloride and one DMSO ligand in axial positions. Coordination of the bidentate ligand occurs via atoms N1 and N5, and DMSO binds via S. An intramolecular hydrogen bond N2−H···O2 is evident in the structure of *cis,cis*-[$Ru^{II}Cl_2(DMSO)_2$(**L1**)] (Figure 1, left). The presence of a proton at N4 is corroborated by the involvement of this atom in hydrogen-bonding interaction with $Cl2^i$ ($i = -x + 1, -y + 1, -z + 2$) [N4···$Cl2^i$ 3.123 Å].

In *mer*-[$Ru^{II}Cl(DMSO)_3$(**L2**−H)], the organic molecule acts as a bidentate monodeprotonated ligand. The site of deprotonation appears to be the atom N2, which does not form short contacts to adjacent molecules. Binding to ruthenium(II) is realized via atoms N1 and N5. The other two positions in the equatorial plane are occupied by the Cl1 ligand and one DMSO, while as axial ligands act two DMSO molecules. All three molecules of DMSO are arranged meridionally and bound to the central atom via S.

Preparation of rHSA Conjugates of 1c−5c. The functionalization of the rHSA protein was carried out using established protocols (see the Experimental Section for full details). The protein was modified with the SHTH linker, which reacts with amine groups on the lysine residues of the protein. Because excess modification of the hydrophobic linkers can result in the precipitation of the protein, the optimal reaction conditions were determined to be within 5-fold stoichiometric excess of the linker molecule. Upon modification, the protein was purified and conjugated with the ruthenium compound (3:1 metal/protein ratio) in PBS (pH 7.4), allowing sample incubation for 6 h at room temperature. The samples were then analyzed by MALDI-TOF-MS. A representative MALDI-TOF-MS spectrum obtained on rHSA samples incubated with **5c** is reported in Figure 2 in comparison to the spectrum of pure rHSA. The reaction of **5c** with the protein appears to be quantitative, and the main peak at about 67 980 Da clearly indicates an increase of approximately 1600 Da with respect to the one of rHSA, most likely corresponding to the presence of about two bound ruthenium moieties.

Cytotoxicity Studies. The antiproliferative activity of all compounds was tested in the human cancer cell lines CH1, SW480, and A549. The IC_{50} values of **1c−5c** were compared to those of [RuCl(μ-Cl)(η^6-arene)]$_2$, free ligands (**L1−L3**), and corresponding [RuCl(η^6-*p*-cymene)(L)]Cl complexes (**1a−5a**; Table 2). It should be noted that, as a general trend, the resulting ruthenium complexes are less cytotoxic than the free ligands. However, the observed antiproliferative effects indicate

dx.doi.org/10.1021/ic201801e | *Inorg. Chem.* 2011, 50, 12669−12679

Table 2. Cytotoxicity of 1c−5c, Compared to [RuCl(μ-Cl)(η⁶-arene)]₂, Free Ligands (L1−L3), and Corresponding [RuCl(η⁶-p-cymene)(L)]Cl Complexes (1a−5a), in Three Human Cancer Cell Lines

compound	IC_{50},[a] μM		
	CH1	SW480	A549
$[RuCl(\mu\text{-}Cl)(\eta^6\text{-arene})]_2$	65 ± 21	215 ± 35	>320
L1[b]	11 ± 3	23 ± 6	29 ± 7
1a[b]	96 ± 18	>320	>320
1c	142 ± 33	>320	>320
L2[b]	1.5 ± 0.6	5.1 ± 1.0	6.7 ± 0.3
2a[b]	21 ± 3	70 ± 8	268 ± 35
2c	32 ± 13	>320	>320
L3[b]	0.63 ± 0.09	0.74 ± 0.26	5.2 ± 0.5
3a[b]	11 ± 1	11 ± 2	68 ± 12
3c	153 ± 42	>320	>320
L4			
4a[c]	9.7 ± 1.6	28 ± 5	32 ± 1
4c	55 ± 15	179 ± 24	>320
L5			
5a[c]	1.9 ± 0.4	1.2 ± 0.5	8.5 ± 0.7
5c	29 ± 2	49 ± 2	123 ± 20

[a]50% inhibitory concentrations (means ± standard deviation from at least three independent experiments), as obtained by the MTT assay (exposure time: 96 h). [b]Taken from ref 25. [c]Taken from ref 21.

a marked selectivity of the ruthenium compounds toward a cancer cell line compared to the ligands **L1**−**L3** (e.g., complex **2c** is more than 10-fold more active in the CH1 cell line than in SW480 and A549 cells). Indeed, the ruthenium complexes showed the strongest effects in the generally quite chemosensitive ovarian carcinoma cell lines CH1, whereas the generally more chemoresistant nonsmall cell lung cancer cell line A549 is the least sensitive to this series of compounds. Concentration−effect curves of **1c**−**5c** and $[RuCl(\mu\text{-}Cl)(\eta^6\text{-arene})]_2$ in the CH1 cells are depicted in Figure S19 in the Supporting Information. While the rank order of the cytotoxicity of the analogous cymene complexes with 3-(1*H*-benzimidazol-2-yl)-1*H*-pyrazolo[3,4-*b*]pyridines is in line with the cytotoxicity of the free ligands, **3a** > **2a** > **1a** corresponding to **L3** > **L2** > **L1**, indicating that both the bromo and methoxymethyl substituents are advantageous for cytotoxic potency, the structure−activity relationship of **1c**−**3c** is less clear-cut, which may be caused by the borderline solubility associated with the presence of the 4-formylphenoxyacetyl-η^6-benzylamide ligand. In the SW480 and A549 cells, complexes **1c**−**3c** show no antiproliferative activity in concentrations up to 320 μM, and neither do **4c** and $[RuCl(\mu\text{-}Cl)(\eta^6\text{-arene})]_2$ in the A549 cells. The most active of the complexes bearing a 4-formylphenoxyacetyl-η^6-benzylamide ligand is the paullone complex **5c** with IC_{50} values of 29 μM in CH1 cells, 49 μM in SW480 cells, and 123 μM in A549 cells. This paullone complex with a derivatized lactam unit (**5c**) shows higher antiproliferative activity than the paullone complex with unmodified lactam group (**4c**) in all three cell lines, as was reported for $[RuCl(\eta^6\text{-}p\text{-cymene})(L)]Cl$ complexes **4a** and **5a** (as well as their osmium analogues) with paullones **L4** and **L5**.[21]

The impact of tethering **1c**−**5c** to rHSA on their antitumor activity in vitro was evaluated in ovarian carcinoma cell line either sensitive (A2780) or resistant to cisplatin (A2780cisR). Table 3 reports the IC_{50} values obtained for inhibition of the

Table 3. Inhibition of Human Ovarian Carcinoma Cell Growth (IC_{50}, μM) for 1c−5c and Their rHSA Conjugates after 72 h of Incubation

compound	IC_{50}, μM	
	A2780	A2780cisR
rHSA	>75[a]	
rHSA−hydrazine	>75[a]	
1c	>200	>200
rHSA−**1c**	45 ± 5	67 ± 3
2c	>200	>200
rHSA-**2c**	43 ± 3	>100
3c	>200	>200
rHSA−**3c**	46 ± 2	69 ± 6
4c	>100	>100
rHSA−**4c**	49 ± 2	43 ± 2
5c	85 ± 4	66 ± 7
rHSA−**5c**	26 ± 2	28 ± 1

[a]Taken from ref 11.

A2780 and A2780cisR cell growth upon treatment with compounds **1c**−**5c** and their rHSA conjugates. As expected from the cytotoxicity data reported above, the ruthenium complexes alone did not significantly affect the cell growth within the tested concentration range, with the most effective being **5c**, whereas a marked response was observed in the case of the rHSA−ruthenium conjugates. In the case of rHSA−**5c**, IC_{50} values of 26 and 28 μM were observed in the two cell lines, indicating that the conjugation strategy overcomes the resistance mechanism that blocks entry and/or increases efflux of cisplatin from the cells.

It is worth mentioning that the potential of macromolecular metal complexes to overcome resistance mechanisms has already been investigated with platinum compounds.[31] In this case, the results showed that albumin binding lowers the cytotoxic activity of platinum complexes in cancer cell lines. However, the HSA−Pt conjugates exhibited comparable activity in the sensitive and cisplatin-resistant cells.

Because the rHSA conjugates contain more than one ruthenium, the increase in the cytotoxicity is not extremely large, but it should be noted that the rHSA conjugates should exploit the so-called "enhanced permeability and retention (EPR)" effect of macromolecules on tumors[32] and, consequently, should selectively accumulate in tumor tissue. The EPR effect is based on the observation that macromolecules are able to penetrate the leaky vasculature surrounding the tumor, and as a result of the increased permeability, the macromolecules "selectively" permeate the tumor tissues compared to the healthy tissues. In addition, the lymphatic drainage system of tumor tissue is impaired, resulting in accumulation of the macromolecules at the tumor site.

Cell Cycle Effects. To study the effects of the compounds on cell cycle distribution in the sensitive ovarian cancer cell line CH1, cells were treated for 24 h, stained with propidium iodide, and analyzed for their DNA content by fluorescence-activated cell sorting (FACS). These experiments revealed that complexes **4c** and **5c** with indolobenzazepine-derived ligands **L4** and **L5**, respectively, induce stronger cell cycle perturbations than **2c** with a pyrazolopyridine-derived ligand (**L2**; Figure 3). In particular, treatment with **5c** caused a pronounced G2/M phase arrest in concentrations up to 80 μM (81 ± 4% of cells in G2/M compared to 36 ± 4% in untreated controls), accompanied by a steady decrease of the G1/G0 fraction, but

dx.doi.org/10.1021/ic201801e | *Inorg. Chem.* 2011, 50, 12669−12679

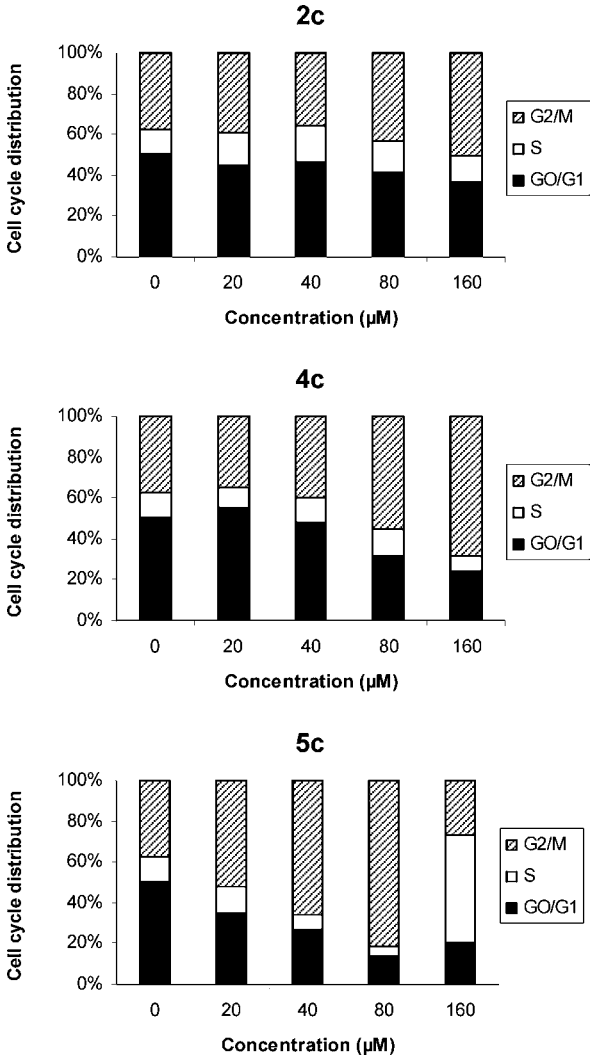

Figure 3. Concentration-dependent impact of **2c**, **4c**, and **5c** on the cell cycle distribution of CH1 cells after exposure for 24 h. The DNA content of cells stained with propidium iodide was analyzed by flow cytometry.

superseded by an S phase arrest at 160 μM (52 ± 0.3% of cells in the S phase). In addition, the appearance of a pronounced sub-G1/G0 fraction (excluded from analysis) and the tremendous decrease of the G2/M fraction (27 ± 6%) at this highest concentration suggest that apoptotic cell death is preferentially induced in G2/M cells. In accordance with the slightly lower cytotoxicity in the MTT assay, **4c** is also somewhat less effective on the cell cycle. Neither an S phase arrest nor a comparable sub-G1/G0 fraction could be observed at the highest concentration, but the compound as well induces a G2/M arrest reaching 68 ± 1% at 160 μM. In conclusion, the differences in the position of the chelating moiety in **4c** and **5c** (whether on the lactam ring or not) seem to merely modulate the antiproliferative potency of the compounds rather than fundamentally change the capacity of inhibiting cell cycle progression.

Final Remarks. Herein we describe the synthesis and characterization of a new series of organometallic complexes of the general formula [RuCl(η^6-arene)(L)]Cl [where L = 3-(1*H*-benzimidazol-2-yl)-1*H*-pyrazolo[3,4-*b*]pyridines and indolo-[3,2-*d*]benzazepines (**L1**−**L5**), which are potential kinase inhibitors]. Complexation of **L1**−**L5** to the ruthenium(II) arene unit yielded compounds with increased solubility in biological media, yet lower, but more selective antiproliferative activity in human cancer cell lines. In order to improve the mild cytotoxic effects of the ruthenium derivatives, we coupled the compounds to serum albumin, which is known to accumulate in tumors. HSA has previously been used to deliver various anticancer drugs such as chlorambucil, doxorubicin, paclitaxel, and cisplatin to cancer cells.[33] Chlorambucil− and paclitaxel−HSA conjugates exhibit cytotoxicity comparable to that of the parent drugs in vitro but are less toxic in vivo,[26,27] and a doxorubicin prodrug using endogenous serum albumin as a drug carrier displays excellent in vivo properties.[34,35]

Thus, the five organometallic complexes were conjugated to rHSA, tethering them to the protein via pH-triggered linkers, as previously described for the organometallic RAPTA compounds that are not cytotoxic but active as antimetastatic agents in vivo.[36−38] MALDI-TOF-MS analysis of the rHSA−Ru adducts showed that typically two ruthenium-containing moieties were bound to the protein. The rHSA conjugates were found to be more cytotoxic than the "free" complexes on human ovarian cancer A2780 cell lines sensitive and resistant to cisplatin. These results are encouraging, and the further development of macromolecular organometallic ruthenium complexes that should selectively target tumor tissue appears to be worthwhile.

■ ASSOCIATED CONTENT

Supporting Information

Synthetic routes to free ligands and [RuCl(μ-Cl)(η^6-arene)]$_2$ (Schemes S1−S3), analytical data of [RuCl(μ-Cl)(η^6-arene)]$_2$ and [RuCl$_2$(η^6-arene)(DMSO)], assigned NMR (^{1}H, ^{13}C, and ^{15}N) signals for **1c**−**5c** and **2c**$_{-HCl}$ compared to [RuCl(μ-Cl)(η^6-arene)]$_2$ and free ligands (Tables S1−S6), sections of the ^{1}H,^{1}H ROESY NMR spectra of **1c**, **4c**, and **5c** (Figures S7−S13), ORTEP views of [RuCl$_2$(η^6-arene)(DMSO)] and **L2**·DMSO (Figures S14 and S15), stability of complexes in solutions, time-dependent UV−vis spectra of complexes in MeOH (**1c**−**5c**) and water (**4c** and **5c**) (Figures S16−S18), concentration−effect curves of **1c**−**5c** and [RuCl(μ-Cl)(η^6-arene)]$_2$ in CH1 cells (Figure S19), and crystallographic data for [RuCl$_2$(η^6-arene)(DMSO)]·0.5H$_2$O, **L2**·DMSO, *cis,cis*-[Ru^{II}Cl$_2$(DMSO)$_2$(**L1**)]·H$_2$O, and *mer*-[Ru^{II}Cl(DMSO)$_3$(**L2**−H)]·H$_2$O in CIF format. This material is available free of charge via the Internet at http://pubs.acs.org.

■ AUTHOR INFORMATION

Corresponding Author

*E-mail: vladimir.arion@univie.ac.at (V.B.A.), paul.dyson@epfl.ch (P.J.D.), bernhard.keppler@univie.ac.at (B.K.K.).

Present Address

⊥Research Institute of Pharmacy, University of Groningen, Antonius Deusinglaan 1, 9713 AV Groningen, The Netherlands.

■ ACKNOWLEDGMENTS

We thank Prof. Markus Galanski for the 2D NMR measurements, Alex Roller for collection of the X-ray data, and the Hertha Firnberg Programme of Austrian Science Fund (Project T 393-N19) for financial support. A.C. thanks the Swiss National Science Foundation (AMBIZIONE Project PZ00P2-136908/1) for funding. Furthermore, we are indebted to Prof.

Verena Dirsch and Daniel Schachner (Institute of Pharmacognosy, University of Vienna, Austria) for providing FACS equipment and technical assistance.

REFERENCES

(1) Haag, R.; Kratz, F. *Angew. Chem., Int. Ed.* **2006**, *45*, 1198−1215.
(2) Brewer, E.; Coleman, J.; Lowman, A. *J. Nanomater.* **2011**, Article ID 408675.
(3) Yokoyama, M. *J. Artif. Organs* **2005**, *8*, 77−84.
(4) Rapoport, N. *Prog. Polym. Sci.* **2007**, *32*, 962−990.
(5) Cho, K.; Wang, X.; Nie, S.; Chen, Z.; Shin, D. M. *Clin. Cancer Res.* **2008**, *14*, 1310−1316.
(6) Haley, B.; Frenkel, E. *Urol. Oncol.* **2008**, *26*, 57−64.
(7) Sanchez-Cano, C.; Hannon, M. J. *Dalton Trans.* **2009**, 10702−10711.
(8) Kratz, F. *J. Controlled Release* **2008**, *132*, 171−183.
(9) Hawkins, M. J.; Soon-Shiong, P.; Desai, N. *Adv. Drug Delivery Rev.* **2008**, *60*, 876−885.
(10) Warnecke, A.; Fichtner, I.; Garmann, D.; Jaehde, U.; Kratz, F. *Bioconjugate Chem.* **2004**, *15*, 1349−1359.
(11) Ang, W. H.; Daldini, E.; Juillerat-Jeanneret, L.; Dyson, P. J. *Inorg. Chem.* **2007**, *46*, 9048−9050.
(12) Ang, W. H.; Casini, A.; Sava, G.; Dyson, P. J. *J. Organomet. Chem.* **2011**, 989−998.
(13) Peacock, A. F. A.; Sadler, P. J. *Chem.—Asian J.* **2008**, *3*, 1890−1899.
(14) Bruijnincx, P. C. A.; Sadler, P. J. *Adv. Inorg. Chem.* **2009**, *61*, 1−62.
(15) Dyson, P. J. *Chimia* **2007**, *61*, 698−703.
(16) Hartinger, C. G.; Dyson, P. J. *Chem. Soc. Rev.* **2009**, *38*, 391−401.
(17) Ang, W. H.; Dyson, P. J. *Eur. J. Inorg. Chem.* **2006**, 4003−4018.
(18) Primik, M. F.; Muehlgassner, G.; Jakupec, M. A.; Zava, O.; Dyson, P. J.; Arion, V. B.; Keppler, B. K. *Inorg. Chem.* **2010**, *49*, 302−311.
(19) Ginzinger, W.; Arion, V. B.; Giester, G.; Galanski, M.; Keppler, B. K. *Cent. Eur. J. Chem.* **2008**, *6*, 340−346.
(20) Schmid, W. F.; John, R. O.; Arion, V. B.; Jakupec, M. A.; Keppler, B. K. *Organometallics* **2007**, *26*, 6643−6652.
(21) Schmid, W. F.; John, R. O.; Muehlgassner, G.; Heffeter, P.; Jakupec, M. A.; Galanski, M.; Berger, W.; Arion, V. B.; Keppler, B. K. *J. Med. Chem.* **2007**, *50*, 6343−6355.
(22) Schmid, W. F.; Zorbas-Seifried, S.; John, R. O.; Arion, V. B.; Jakupec, M. A.; Roller, A.; Galanski, M.; Chiorescu, I.; Zorbas, H.; Keppler, B. K. *Inorg. Chem.* **2007**, *46*, 3645−3656.
(23) Dobrov, A.; Arion, V. B.; Kandler, N.; Ginzinger, W.; Jakupec, M. A.; Rufinska, A.; Graf von Keyserlingk, N.; Galanski, M.; Kowol, C.; Keppler, B. K. *Inorg. Chem.* **2006**, *45*, 1945−1950.
(24) Filak, L. K.; Muehlgassner, G.; Jakupec, M. A.; Heffeter, P.; Berger, W.; Arion, V. B.; Keppler, B. K. *J. Biol. Inorg. Chem.* **2010**, *15*, 903−918.
(25) Stepanenko, I. N.; Novak, M. S.; Mühlgassner, G.; Roller, A.; Hejl, M.; Arion, V. B.; Jakupec, M. A.; Keppler, B. K. *Inorg. Chem.* **2011**, *50*, 11715−11728.
(26) Dosio, F.; Brusa, P.; Crosasso, P.; Arpicco, S.; Cattel, L. *J. Controlled Release* **1997**, *47*, 293−304.
(27) Kratz, F.; Beyer, U.; Roth, T.; Schutte, M. T.; Unold, A.; Fiebig, H. H.; Unger, C. *Arch. Pharm.* **1998**, *331*, 47−53.
(28) *SAINT-Plus*, version 7.06a, and *APEX2*; Bruker-Nonius AXS Inc.: Madison, WI, 2004.
(29) Sheldrick, G. M. *Acta Crystallogr.* **2008**, *A64*, 112−122.
(30) Johnson, G. K. Report ORNL-5138; Oak Ridge National Laboratory: Oak Ridge, TN, 1976.
(31) Garmann, D.; Warnecke, A.; Kalayda, G. V.; Kratz, F.; Jaehde, U. *J. Controlled Release* **2008**, *131*, 100−106.
(32) Modi, S.; Jain, J. P.; Domb, A. J.; Kumar, N. *Curr. Pharm. Des.* **2006**, *12*, 4785−4796.
(33) Chuang, V. T. G.; Kragh-Hansen, U.; Otagiri, M. *Pharm. Res.* **2002**, *19*, 569−577.
(34) Kratz, F.; Muller-Driver, R.; Hofmann, I.; Drevs, J.; Unger, C. *J. Med. Chem.* **2000**, *43*, 1253−1256.
(35) Kratz, F.; Warnecke, A.; Scheuermann, K.; Stockmar, C.; Schwab, J.; Lazar, P.; Druckes, P.; Esser, N.; Drevs, J.; Rognan, D.; Bissantz, C.; Hinderling, C.; Folkers, G.; Fichtner, I.; Unger, C. *J. Med. Chem.* **2002**, *45*, 5523−5533.
(36) Scolaro, C.; Bergamo, A.; Brescacin, L.; Delfino, R.; Cocchietto, M.; Laurenczy, G.; Geldbach, T. J.; Sava, G.; Dyson, P. J. *J. Med. Chem.* **2005**, *48*, 4161−4171.
(37) Bergamo, A.; Masi, A.; Dyson, P. J.; Sava, G. *Int. J. Oncol.* **2008**, *33*, 1281−1289.
(38) Chatterjee, S.; Kundu, S.; Bhattacharyya, A.; Hartinger, C. G.; Dyson, P. J. *J. Biol. Inorg. Chem.* **2008**, *13*, 1149−1155.